

Effect of energy deposited by cosmic-ray particles on interferometric gravitational wave detectors

Kazuhiro Yamamoto,* Hideaki Hayakawa, Atsushi Okada, Takashi Uchiyama, Shinji Miyoki, Masatake Ohashi, and Kazuaki Kuroda
*Institute for Cosmic Ray Research, the University of Tokyo,
 5-1-5 Kashiwa-no-Ha, Kashiwa, Chiba 277-8582, Japan*

Nobuyuki Kanda

Department of Physics, Osaka City University, 3-3-138 Sugimoto, Sumiyoshi-ku, Osaka, Osaka 558-8585, Japan

Daisuke Tatsumi and Yoshiki Tsunesada

National Astronomical Observatory of Japan, 2-21-1 Osawa, Mitaka, Tokyo 181-8588, Japan

(Dated: November 18, 2018)

We investigated the noise of interferometric gravitational wave detectors due to heat energy deposited by cosmic-ray particles. We derived a general formula that describes the response of a mirror against a cosmic-ray passage. We found that there are differences in the cosmic-ray responses (the dependence of temperature and cosmic-ray track position) in cases of interferometric and resonant gravitational wave detectors. The power spectral density of vibrations caused by low-energy secondary muons is 100-times smaller than the goal sensitivity of future second-generation interferometer projects, such as LCGT and Advanced LIGO. The arrival frequency of high-energy cosmic-ray muons that generate enough large showers inside mirrors of LCGT and Advanced LIGO is one per a millennium. We also discuss the probability of exotic-particle detection with interferometers.

PACS numbers: 04.80.Nn, 95.35.+d, 95.55.Vj, 95.85.Ry

I. INTRODUCTION

Recent improvements of the sensitivity and operational stability of gravitational wave detectors is remarkable. Observation runs have already been performed in several interferometer (LIGO [1], VIRGO [2], GEO [3], TAMA [4], CLIO [5]) and resonator (ALLEGRO [6], EXPLORER [7], NAUTILUS [8], AURIGA [9], NIOBE [10], MARIO SCHENBERG [11]) projects. In order of gravitational wave detection, the reduction of noise and fake triggers is crucial, since the gravitational wave amplitude and number of events are expected to be small and rare. In 1969, it was pointed out that cosmic-ray particles could cause fake triggers in resonators [12]. The interpretation of excitations of resonators by cosmic-ray particles is follows: The heat energy deposited by cosmic-ray particle passages induces temperature gradients around their tracks, and thermal stress excites internal vibrations of the resonator. These phenomena have been investigated, for example, observations of excited resonator vibrations by beams from accelerators [13, 14], simultaneous detection of resonator excitation and cosmic-ray particles [15], and studies of exotic events in super-conductive resonators [16, 17, 18]. In some research, resonators were also operated and treated as exotic-particle detectors [19, 20, 21, 22]. These studies suggest that cosmic-ray

heating is a possible noise source in interferometric detectors [23, 24, 25, 26] (other effects on interferometers, the momentum and electrical charge brought by cosmic-ray particles, are discussed in Refs. [23, 24, 25, 27]).

We investigated details of this effect by cosmic-ray energy deposition in interferometers. A formula that describes the response of a mirror against a cosmic-ray passage was derived. This formula reveals differences between the cosmic-ray responses of interferometers and resonators. We used it to evaluate the amplitude of vibrations caused by cosmic-ray particles in typical cases of interferometers, and examined the effect in gravitational wave detection. We also considered the probability of exotic-particle detection with interferometers.

II. FORMULA OF EXCITED MOTION BY A COSMIC-RAY PARTICLE

A. Outline of derivation of the formula

In order to simplify the discussion, the mirror vibration excited by a cosmic-ray particle is investigated. A vibration excited by many particles, like a shower, is a superposition of that by one particle. The excitation by a particle is considered under the following assumptions. The particle goes straight and never stops in the mirror. Its speed is faster than that of sound in the mirror. A long and narrow heated volume appears at the instant of particle passage.

The heat-conduction equation is solved in order to calculate the time evolution of the temperature gradient.

*Electronic address: kazuhiro.yamamoto@aei.mpg.de; Present address: Max Planck Institute for Gravitational Physics, Albert Einstein Institute, Callinstrasse 38, D-30167 Hannover, Germany.

The vibration of the mirror is examined using the equation of motion of an elastic body with thermal stress, which is proportional to the thermal gradient.

B. Formula

Since the heated volume is smaller than that of the mirror, itself [28, 29], the mirror and the initial heated volume are treated as an infinite body and a line, respectively. The direction of the cosmic-ray track is taken as the z -axis. The heat-conduction equation is described as [30]

$$\frac{\partial}{\partial t}\delta T - \frac{\kappa}{\rho C}\Delta(\delta T) = \frac{1}{\rho C}\frac{dE}{dl}\delta(x)\delta(y)\delta(t), \quad (1)$$

where δT is the temperature difference caused by a cosmic-ray particle. The quantities κ, ρ, C and dE/dl are the thermal conductivity, density, specific heat per unit mass, and energy loss of a particle per unit length, respectively. The solution is described as [31]

$$\delta T = \frac{1}{4\pi\kappa t}\frac{dE}{dl}\exp\left[-\frac{\rho C}{4\kappa t}(x^2 + y^2)\right]. \quad (2)$$

The radius of the heated volume increases with time due to conduction. The time when the heated area radius becomes a is

$$\tau_a = \frac{\rho C a^2}{4\kappa}. \quad (3)$$

The equation of motion of an elastic body with thermal stress is described as [30]

$$\begin{aligned} \rho\frac{\partial^2\mathbf{u}}{\partial t^2} - \frac{Y}{2(1+\sigma)}\Delta\mathbf{u} - \frac{Y}{2(1+\sigma)(1-2\sigma)}\text{grad div}\mathbf{u} \\ = -\frac{Y\alpha}{1-2\sigma}\text{div}\delta T, \end{aligned} \quad (4)$$

where \mathbf{u} represents the displacement of a volume element in the elastic body. The quantities Y, σ and α are Young's modulus, the Poisson ratio, and the linear thermal-expansion coefficient, respectively. By substituting Eq. (2) for Eq. (4), we obtain the output of a interferometer X ,

$$X = \int_{\text{surface}} u_{\text{opt}}(\mathbf{r})P(\mathbf{r})dS, \quad (5)$$

where u_{opt} is the optical axis component of \mathbf{u} and P is the intensity profile of the laser beam,

$$P(\mathbf{r}) = \frac{2}{\pi r_0^2}\exp\left(-\frac{2r^2}{r_0^2}\right). \quad (6)$$

The quantities r and r_0 are the distance from the optical axis and the beam radius. We employ the modal expansion method [32, 33, 34] to calculate \mathbf{u} and X . In this

method, \mathbf{u} and X are represented by a superposition of the resonant mode displacement,

$$\mathbf{u}(\mathbf{r}, t) = \sum_n \mathbf{w}_n(\mathbf{r})q_n(t), \quad (7)$$

$$X(t) = \sum_n q_n(t), \quad (8)$$

where \mathbf{w}_n and q_n represent the displacement and time development of the n -th resonant mode, respectively. These basis functions are normalized to satisfy a condition [33, 34],

$$\int_{\text{surface}} w_{n,\text{opt}}(\mathbf{r})P(\mathbf{r})dS = 1, \quad (9)$$

where $w_{n,\text{opt}}$ is the optical axis component of \mathbf{w}_n . The equation of motion of each mode is the same as that of a harmonic oscillator,

$$-m_n\omega_n^2\tilde{q}_n(\omega) + m_n\omega_n^2[1 + i\phi_n(\omega)]\tilde{q}_n(\omega) = \tilde{F}_n(\omega), \quad (10)$$

in the frequency domain. The quantity ϕ_n is the loss angle, which represents dissipation of the n -th mode [32]. The force F_n applied on the n -th mode is related to the thermal stress. The quantities m_n and ω_n are the effective mass and the resonant angular frequency [33, 34]. The effective mass is defined as

$$m_n = \int_{\text{volume}} \rho\mathbf{w}_n(\mathbf{r}) \cdot \mathbf{w}_n(\mathbf{r})dV. \quad (11)$$

The quantities $\tilde{q}_n(\omega)$ and $\tilde{F}_n(\omega)$ are the Fourier components of q_n and F_n , respectively:

$$\tilde{X}(\omega) = \frac{1}{2\pi}\int_{-\infty}^{\infty} X(t)\exp(-i\omega t)dt, \quad (12)$$

$$X(t) = \int_{-\infty}^{\infty} \tilde{X}(\omega)\exp(i\omega t)d\omega. \quad (13)$$

The force F_n is obtained from the modal decomposition of the thermal stress on the right-hand side of Eq. (4). The decomposition procedure [33, 34] is as follows. The thermal-stress term is multiplied by \mathbf{w}_n . The integral of this inner product over all the volume is F_n . This force F_n decreases after the heated volume scale, a , becomes larger than the n -th mode wavelength. In order to simplify the discussion, it is assumed that the time evolution of F_n [19, 35] is expressed as

$$F_n(t) = \begin{cases} F_n(0)\exp\left(-\frac{t}{\tau_n}\right) & (t > 0) \\ 0 & (t < 0) \end{cases}. \quad (14)$$

The quantities $F_n(0)$ and τ_n are the initial value and the decay time of the force, respectively. The initial value, $F_n(0)$, is written as [20, 36]

$$F_n(0) = \frac{Y\alpha}{1-2\sigma}\frac{1}{\rho C}\left(\int \text{div}\mathbf{w}_n dl\right)\frac{dE}{dl}. \quad (15)$$

The integral along the cosmic-ray track represents the coupling between the thermal stress and the n -th mode. The coefficient $1/(\rho C)$ is a factor used to transform the heat energy into the temperature gradient. The force F_n is described as a product of the temperature gradient and $Y\alpha/(1-2\sigma)$. From Eq. (3), the time τ_n when the heated volume radius becomes comparable to the wavelength of the n -th mode is expressed as

$$\tau_n = \frac{\rho C \lambda_n^2}{4\kappa} = \frac{\pi^2 \rho C v^2}{\kappa \omega_n^2} \sim \frac{\pi^2 Y C}{\kappa \omega_n^2}. \quad (16)$$

The quantities λ_n and v are the wavelength and sound velocity:

$$\lambda_n = \frac{2\pi v}{\omega_n}, \quad (17)$$

$$v \sim \sqrt{\frac{Y}{\rho}}. \quad (18)$$

The Fourier component of F_n in Eq. (14) is written in the form

$$\tilde{F}_n(\omega) = \frac{F_n(0)}{2\pi} \frac{\tau_n}{1 + i\omega\tau_n}. \quad (19)$$

We now write down the formula of the mirror vibration excited by a cosmic-ray particle using Eqs. (8), (10), (15) and (19):

$$\begin{aligned} \tilde{X}(\omega) &= \sum_n \tilde{q}_n(\omega) \\ &= \sum_n \frac{\tilde{F}_n(\omega)}{-m_n\omega^2 + m_n\omega_n^2(1 + i\phi_n)} \\ &= \frac{1}{2\pi} \frac{Y\alpha}{1-2\sigma} \frac{1}{\rho C} \frac{dE}{dl} \\ &\quad \times \sum_n \frac{1}{-m_n\omega^2 + m_n\omega_n^2(1 + i\phi_n)} \frac{\tau_n}{1 + i\omega\tau_n} \\ &\quad \times \left(\int \text{div} \mathbf{w}_n dl \right). \end{aligned} \quad (20)$$

C. Frequency dependence of the formula

A schematic view of the frequency dependence of the modes $\tilde{q}_n(\omega)$ in Eq. (20) is shown in Fig. 1. Here, we discuss the frequency dependence below the resonant frequencies of the mirrors, because the observation band of interferometers (around 100 Hz) is below the fundamental mode (the order of 10 kHz). The cut-off frequency, $1/(2\pi\tau_n)$, is extremely smaller than the resonant frequency, $\omega_n/(2\pi)$, as shown in Fig. 1, because sound is generally faster than heat conduction. The absolute value $|\tilde{q}_n(\omega)|$ is inversely proportional to the frequency between $1/(2\pi\tau_n)$ and $\omega_n/(2\pi)$. Below the cut-off frequency, $1/(2\pi\tau_n)$, $|\tilde{q}_n(\omega)|$ is constant.

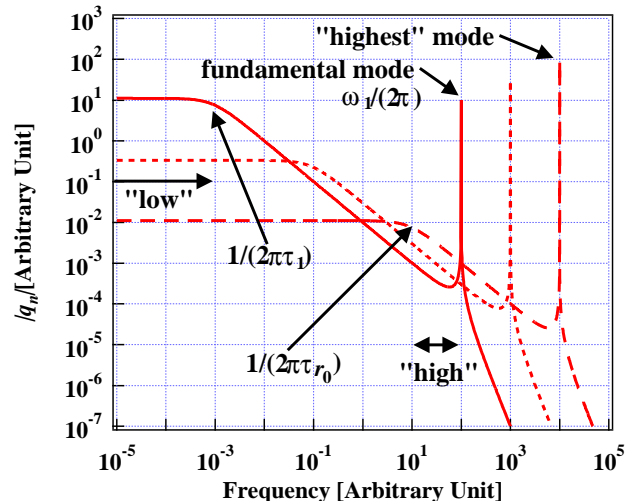


FIG. 1: A schematic view of the frequency dependence of the Fourier components of mode motion excited by a cosmic-ray particle, $\tilde{q}_n(\omega)$ in Eq. (20). The absolute value $|\tilde{q}_n(\omega)|$ is inversely proportional to the frequency between $1/(2\pi\tau_n)$ and $\omega_n/(2\pi)$. Below the cut-off frequency, $1/(2\pi\tau_n)$, it is constant. The "highest" mode is that with a wavelength comparable to the beam radius, r_0 , and contributions of higher modes are negligible in the summation of Eq. (20) [37, 38]. The cut-off frequency of the "highest" mode, $1/(2\pi\tau_{r_0})$, is smaller than the fundamental mode resonant frequency, $\omega_1/(2\pi)$, in general. The cut-off frequency, $1/(2\pi\tau_n)$, of the lower mode is smaller. In the range between $1/(2\pi\tau_{r_0})$ and $\omega_1/(2\pi)$ (the "high" frequency region in this graph), $|\tilde{X}(\omega)| = |\sum \tilde{q}_n(\omega)|$ is inversely proportional to the frequency. Below the cut-off frequency of the fundamental mode, $1/(2\pi\tau_1)$ (the "low" frequency region in this graph), $|\tilde{X}(\omega)|$ is independent of the frequency. The approximation formulae in the "high" and "low" frequency regions, Eqs. (30) and (34), are derived using Eq. (20).

The frequency dependence of $\tilde{X}(\omega) = \sum \tilde{q}_n(\omega)$ is as follows. The "highest" mode in Fig. 1 is that with a wavelength comparable to the beam radius, r_0 , and contributions of higher modes are negligible in the summation of Eq. (20) [37, 38]. The thermal relaxation time, τ_{r_0} , for this "highest" mode is described as

$$\tau_{r_0} = \frac{\rho C r_0^2}{4\kappa} \quad (21)$$

from Eq. (16). The cut-off frequency of the "highest" mode, $1/(2\pi\tau_{r_0})$, is smaller than the fundamental mode resonant frequency, $\omega_1/(2\pi)$, in general, as shown in Fig. 1. The cut-off frequency, $1/(2\pi\tau_n)$, of the lower mode is smaller from Eq. (16). In the range between $1/(2\pi\tau_{r_0})$ and $\omega_1/(2\pi)$ (the "high" frequency region in Fig. 1), $|\tilde{X}(\omega)| = |\sum \tilde{q}_n(\omega)|$ is inversely proportional to the frequency. Below the cut-off frequency of the fundamental mode, $1/(2\pi\tau_1)$ (the "low" frequency region in Fig. 1), $|\tilde{X}(\omega)|$ is independent of the frequency. From Eq. (16),

the relaxation time, τ_1 , is described as

$$\tau_1 = \frac{\rho C \lambda_1^2}{4\kappa} = \frac{\rho C R^2}{\kappa}, \quad (22)$$

because the wavelength of the fundamental mode, λ_1 , is comparable to the mirror diameter, $2R$.

The typical values of $|\tilde{X}(\omega)|$ in the "high" and "low" frequency regions of Fig. 1 are evaluated using Eq. (20). In the "high" frequency region, $1/(2\pi\tau_{r_0}) < f < \omega_1/(2\pi)$, it is approximated as ($|\phi_n| \ll 1$ in usual cases)

$$|\tilde{X}(\omega)| \sim \frac{1}{2\pi} \frac{Y\alpha}{1-2\sigma} \frac{1}{\rho C} \frac{dE}{dl} \frac{1}{\omega} \left| \sum_n \frac{1}{m_n \omega_n^2} \int \text{div} \mathbf{w}_n dl \right|, \quad (23)$$

$1/(2\pi\tau_{r_0}) < f < \omega_1/(2\pi)$.

The sign of the integral in Eq. (23) depends on the modes. The typical absolute value of the summation in Eq. (23) is evaluated as the square root of a summation of squares of the terms. Equation (23) is rewritten as

$$|\tilde{X}(\omega)| \sim \frac{1}{2\pi} \frac{Y\alpha}{1-2\sigma} \frac{1}{\rho C} \frac{dE}{dl} \frac{1}{\omega} \times \sqrt{\sum_n \frac{1}{m_n^2 \omega_n^4} \left(\int \text{div} \mathbf{w}_n dl \right)^2}, \quad (24)$$

$1/(2\pi\tau_{r_0}) < f < \omega_1/(2\pi)$.

The integral along the cosmic-ray track in Eq. (24) is evaluated as follows. The average of the length of the cosmic-ray track is comparable to the radius of the mirror, R . The average of $|\mathbf{w}_n|^2$, $\langle |\mathbf{w}_n|^2 \rangle$, is related to Eq. (11),

$$m_n = \int \rho |\mathbf{w}_n|^2 dV = M \langle |\mathbf{w}_n|^2 \rangle, \quad (25)$$

where M is the mass of the mirror. This equation gives

$$\sqrt{\langle |\mathbf{w}_n|^2 \rangle} = \sqrt{\frac{m_n}{M}}. \quad (26)$$

The divergence of \mathbf{w}_n in Eq. (24) can be represented by the product of \mathbf{w}_n and the wavenumber ω_n/v , because \mathbf{w}_n is the basis of the solution of the wave equation. Consequently, Eq. (24) is described as

$$|\tilde{X}(\omega)| \sim \frac{1}{2\pi} \frac{Y\alpha}{1-2\sigma} \frac{1}{\rho C} \frac{dE}{dl} \frac{R}{v\sqrt{M}} \frac{1}{\omega} \sqrt{\sum_n \frac{1}{m_n \omega_n^2}}, \quad (27)$$

$1/(2\pi\tau_{r_0}) < f < \omega_1/(2\pi)$.

The summation in Eq. (27) is the same as the response of a mirror against a static force [39, 40],

$$\sum_n \frac{1}{m_n \omega_n^2} = \frac{1-\sigma^2}{\sqrt{\pi} Y r_0}. \quad (28)$$

In order to simplify the discussion, the relation

$$M = \pi \rho R^3 \quad (29)$$

is assumed. The radius of the mirror, R , is nearly equal to its thickness, H , in usual cases of interferometric gravitational wave detectors. Using Eqs. (18), (28) and (29), Eq. (27) is written in the form

$$|\tilde{X}(\omega)| \sim \frac{1}{2\pi^{7/4}} \frac{\alpha \sqrt{1-\sigma^2}}{1-2\sigma} \frac{1}{\rho C} \frac{dE}{dl} \frac{1}{\sqrt{R} r_0} \frac{1}{\omega}, \quad (30)$$

$1/(2\pi\tau_{r_0}) < f < \omega_1/(2\pi)$.

Equation (20) in the "low" frequency band of Fig. 1 is evaluated in the same manner as in the previous paragraph. Using Eq. (16), the result is written as

$$|\tilde{X}(\omega)| \sim \frac{1}{2\pi} \frac{Y\alpha}{1-2\sigma} \frac{1}{\rho C} \frac{dE}{dl} \times \sqrt{\sum_n \frac{\tau_n^2}{m_n^2 \omega_n^4} \left(\int \text{div} \mathbf{w}_n dl \right)^2} \sim \frac{\sqrt{\pi}}{2} \frac{Y^{3/2} \alpha}{1-2\sigma} \frac{1}{\rho \kappa} \frac{dE}{dl} \frac{1}{\sqrt{R}} \sqrt{\sum_n \frac{1}{m_n \omega_n^6}}, \quad (31)$$

$f < 1/(2\pi\tau_1)$.

It can be seen that only the fundamental mode is dominant, because of the frequency dependence of ω_n^6 . The quantities of this mode are as follows [20, 37]:

$$m_1 \sim \frac{M}{2} \sim \frac{\pi \rho R^3}{2}, \quad (32)$$

$$\omega_1 \sim \frac{\pi}{H} \sqrt{\frac{Y}{\rho}} \sim \frac{\pi}{R} \sqrt{\frac{Y}{\rho}}. \quad (33)$$

Equation (31) is expressed as

$$|\tilde{X}(\omega)| \sim \frac{1}{\sqrt{2}\pi^3} \frac{\alpha}{1-2\sigma} \frac{1}{\kappa} \frac{dE}{dl} R, \quad f < 1/(2\pi\tau_1). \quad (34)$$

D. Formula in time domain

Here, we discuss the excitation formula Eq. (20) in the time domain. Only a contribution of the n -th mode is considered in order to simplify the discussion. If the Q -value, $Q_n = 1/\phi_n(\omega_n)$, is larger than unity and $1/\tau_n$ is smaller than ω_n , q_n in the time domain ($t > 0$) is written in a form

$$q_n(t) \sim \frac{F_n(0)}{m_n \omega_n^2} \exp\left(-\frac{t}{\tau_n}\right) - \frac{F_n(0)}{m_n \omega_n^2} \cos(\omega_n t) \exp\left(-\frac{\omega_n t}{2Q_n}\right). \quad (35)$$

Figure 2 shows the fundamental mode, q_1 , in the time domain.

The second term in Eq. (35) is dominated by $\tilde{X}(\omega)$ near the resonant frequency. This is the excited resonant vibration and its decay. The outputs of resonant detectors are described with this term. The first term in Eq.

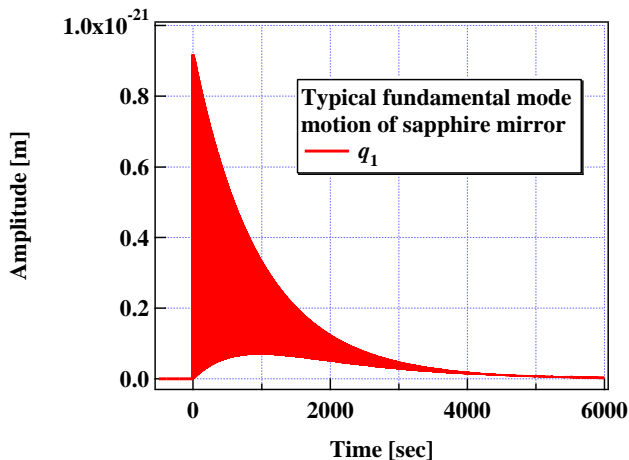


FIG. 2: Vibration of the fundamental mode caused by a low-energy cosmic-ray muon in the time domain, q_1 in Eq. (35). In the calculation, the material values of sapphire at room temperature are used. Since the Q-value is extremely high, i.e. the decay time is longer than the period of the resonant motion, we are not able to see the resonant motion of the one period in this graph.

(35) represents the drift of the center of the resonant vibration caused by the relaxation of thermal stress. This is dominated by $\tilde{X}(\omega)$ below the fundamental mode. The outputs of interferometric detectors are described with this term.

The initial amplitude of $\sum_n 2F_n(0)/(m_n\omega_n^2)$ is evaluated as Eq. (30),

$$\begin{aligned} \sum_n \frac{2F_n(0)}{m_n\omega_n^2} &= \frac{2}{\pi^{3/4}} \frac{\alpha\sqrt{1-\sigma^2}}{1-2\sigma} \frac{1}{\rho C} \frac{dE}{dl} \frac{1}{\sqrt{Rr_0}} \\ &= 6.4 \times 10^{-21} \text{ m} \left(\frac{\alpha}{5 \times 10^{-6} \text{ /K}} \right) \\ &\quad \times \left(\frac{1}{2.3} \frac{\sqrt{1-\sigma^2}}{1-2\sigma} \right) \\ &\quad \times \left(\frac{7.9 \times 10^2 \text{ J/kg/K}}{C} \right) \\ &\quad \times \left(\frac{1}{2 \text{ MeV/(g cm}^{-2})} \frac{1}{\rho} \frac{dE}{dl} \right) \left(\frac{25 \text{ cm}}{2R} \right)^{1/2} \\ &\quad \times \left(\frac{3 \text{ cm}}{r_0} \right)^{1/2}. \end{aligned} \quad (36)$$

Here, we consider a sapphire mirror at room temperature.

III. DISCUSSION ABOUT THE FORMULA

A. Effect on low-temperature interferometers

In some future projects using interferometric detectors as LCGT [41] and ET [42], mirrors will be cooled in order

to reduce the thermal noise (for example, LCGT mirrors at 20 K). In the quantities of the force, F_n , which is related to the thermal stress, α , C and κ in Eqs. (15) and (16) strongly depend on the temperature [43]. The initial value of the force, $F_n(0)$ in Eq. (15), is proportional to α/C . The decay time of the force, τ_n in Eq. (16), is proportional to C/κ . The Grüneisen relation [44] predicts that the ratio α/C is independent of the temperature. The initial force, $F_n(0)$, and the initial amplitude of the excited vibration do not depend on temperature. On the contrary, in the case of crystals, the decay time, τ_n ($\propto C/\kappa$), of the first term in Eq. (35) is extremely short at the cryogenic temperature, because of the small C and large κ . The cut-off frequency, $1/(2\pi\tau_n)$, in the low-temperature region is higher than that at room temperature (e.g. Ref. [26]). For example, the cut-off frequencies of sapphire at room temperature, obtained from Eqs. (21) and (22), are:

$$\begin{aligned} \frac{1}{2\pi\tau_1} &= 0.13 \text{ mHz} \left(\frac{4 \text{ g/cm}^3}{\rho} \right) \left(\frac{7.9 \times 10^2 \text{ J/kg/K}}{C} \right) \\ &\quad \times \left(\frac{25 \text{ cm}}{2R} \right)^2 \left(\frac{\kappa}{40 \text{ W/m/K}} \right), \end{aligned} \quad (37)$$

$$\begin{aligned} \frac{1}{2\pi\tau_{r_0}} &= 9.0 \text{ mHz} \left(\frac{4 \text{ g/cm}^3}{\rho} \right) \left(\frac{7.9 \times 10^2 \text{ J/kg/K}}{C} \right) \\ &\quad \times \left(\frac{3 \text{ cm}}{r_0} \right)^2 \left(\frac{\kappa}{40 \text{ W/m/K}} \right). \end{aligned} \quad (38)$$

The values at 20 K are:

$$\begin{aligned} \frac{1}{2\pi\tau_1} &= 58 \text{ Hz} \left(\frac{4 \text{ g/cm}^3}{\rho} \right) \left(\frac{0.69 \text{ J/kg/K}}{C} \right) \\ &\quad \times \left(\frac{25 \text{ cm}}{2R} \right)^2 \left(\frac{\kappa}{1.6 \times 10^4 \text{ W/m/K}} \right), \end{aligned} \quad (39)$$

$$\begin{aligned} \frac{1}{2\pi\tau_{r_0}} &= 4.0 \text{ kHz} \left(\frac{4 \text{ g/cm}^3}{\rho} \right) \left(\frac{0.69 \text{ J/kg/K}}{C} \right) \\ &\quad \times \left(\frac{3 \text{ cm}}{r_0} \right)^2 \left(\frac{\kappa}{1.6 \times 10^4 \text{ W/m/K}} \right). \end{aligned} \quad (40)$$

At low temperature, the cut-off frequencies are near the observation band of gravitational wave detectors (around 100 Hz). The "high" frequency approximation of $|\tilde{X}(\omega)|$ in Eq. (30) is only appropriate for room-temperature interferometers, and not valid for cryogenic interferometers. In order to show the effect of the cooling mirrors, $|\tilde{q}_1(\omega)|$ of a sapphire mirror at 300 K and 20 K are plotted in Fig. 3. In the low-frequency region, $\tilde{X}(\omega)$ becomes much smaller due to cooling. The "low" frequency approximation of $|\tilde{X}(\omega)|$ in Eq. (34) is proportional to $\alpha/\kappa = \alpha/C \times C/\kappa \propto C/\kappa$, which is small in the low-temperature region. Since the decay time of the force F_n becomes shorter, it is difficult to excite the low-frequency component. The Fourier components $|\tilde{q}_1(\omega)|$ in the high-frequency region of Fig. 3 are comparable in the cases

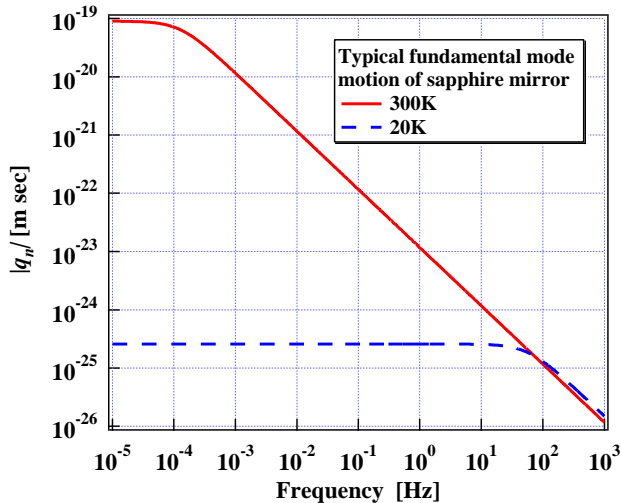


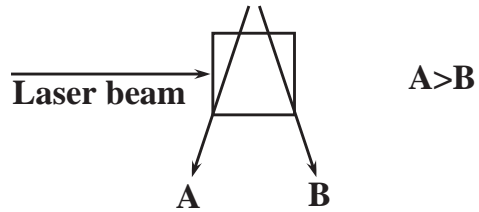
FIG. 3: Fourier components of the fundamental mode motion, $|\tilde{q}_1(\omega)|$, of a sapphire mirror excited by a low-energy cosmic-ray muon at 300 K (solid line) and 20 K (dashed line). The cut-off frequency, $1/(2\pi\tau_1)$, at 20 K is higher than that at 300 K. The mirror cooling reduces the low-frequency component because the decay time of F_1 , which is related to the thermal stress, is shorter. The higher frequency component is independent of temperature because of the Grüneisen relation [44].

of 20 K and 300 K. The "high" frequency approximation of $|\tilde{X}(\omega)|$ in Eq. (30) is independent of temperature because it is proportional to α/C and related to the first term of Eq. (35) at $t \sim 0$. From the cut-off frequencies in Eqs. (39) and (40) and a comparison between Eq. (34) at 20 K and Eq. (30), it can be seen that the vibration of a cooled sapphire mirror excited by a cosmic-ray particle in the observation band (around 100 Hz) is a few-times smaller than that at room temperature. This is an advantage of cryogenic interferometers in addition to the suppression of the thermal noise [45, 46, 47], thermal lensing effect [48] and parametric instability [49]. It must be noted that motions excited by cosmic-ray particles in resonant detectors are independent of temperature [16, 17, 18]. This is because the initial amplitude, the second term of Eq. (35) at $t \sim 0$, does not depend on temperature.

B. Cosmic-ray track position dependence

In the calculation of Eq. (20), the signs of the integral terms in the summation are important. The sign depends on the positions of a cosmic-ray track and the laser beam spot, because the displacement of the mode w_n is normalized to satisfy Eq. (9) [50]. If the particle track is near the beam spot, the signs of the integrals of many modes are the same, because the basis functions, w_n , on the track are similar. If the track is far from the spot, w_n on the track and the integral signs are different

Interferometer



Bar resonator

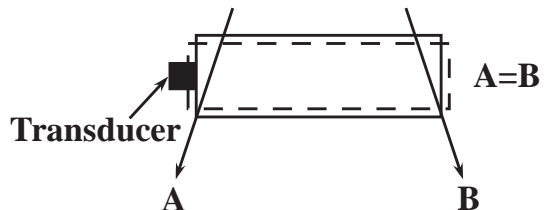


FIG. 4: Track position dependence of the cosmic-ray heating effect of interferometers and bar resonators. In the outputs of interferometers, the vibration caused by a particle that goes along track A near the beam spot is larger than that along track B far from the beam spot. On the contrary, in the case of bars, the vibration by track A is the same as that by track B because the displacement of the resonant modes is symmetric or antisymmetric with respect to the center of the bar. The dashed line shows the fundamental mode deformation.

for various modes. Since the sign of q_n in Eq. (20) below the fundamental mode is the same as that of the integral, $|\tilde{X}(\omega)|$ below the first mode is larger and smaller if the cosmic-ray track is near and far from the beam spot, respectively. Another explanation about the cosmic-ray track position dependence is as follows. The heated volume on the particle track pushes around them. Since the center of the mirror does not move because of the conservation of momentum, a larger motion is observed if the track is near the beam spot. The track position dependence of the cosmic-ray heating effect in interferometers is different from that in bar resonators, as shown in Fig. 4. In the outputs of bars, the vibration caused by a particle that goes along track A in Fig. 4 is the same as that along track B, because the displacement of the resonant modes is symmetric or antisymmetric with respect to the center of the bar (the dashed line in Fig. 4 shows the fundamental mode deformation). The difference between interferometers and the bar resonators is related to the number of modes to be considered. In the case of bars, only the fundamental mode is taken into account. On the other hand, in the case of interferometers, many modes contribute to the response of a mirror. The signs of these modes have an important role. The discussion above is the same as that about thermal noise below the fundamental mode caused by inhomogeneously distributed loss [33, 34, 51].

IV. APPLICATION I — LOW-ENERGY COSMIC-RAY PARTICLES

A. Low-energy cosmic-ray particles and interaction with matter

Primary cosmic rays generate extensive air showers in the atmosphere. Cosmic-ray particles on the ground are secondaries from air showers. Three quarters of secondary particles at sea-level are muons. The remainder are almost electrons [52]. Muons with small energy (less than about 0.22 GeV) and electrons can be neglected because it is difficult to penetrate matter around the mirrors, for example, walls of buildings, vacuum chambers [52]. The speed of muons that arrive at the mirrors is comparable to that of light. The flux of these cosmic-ray muons at sea-level is about 2×10^{-2} /cm²/sec [52, 53].

Since the number of higher energy muons is smaller [54], the energy of most of the cosmic-ray muons is below 100 GeV. In this low-energy region, the dissipation process in material is dominated by ionization [54, 55], which is Coulomb scattering with electrons in atoms of matter [55]. The ionization loss is about

$$\frac{1}{\rho} \frac{dE}{dl} = 2 \text{ MeV}/(\text{g cm}^{-2}), \quad (41)$$

and almost independent of the particle energies [54, 55]. The typical loss per unit length, dE/dl , is several MeV/cm.

The effect of mirror excitation by cosmic-ray particles depends on the arrival frequency of particles and the decay time of the vibrations. If the decay time is longer than the interval of the particle arrivals, the mirror vibration is maintained. If the next muon comes after the vibration has disappeared, the vibration can be treated as a burst event. The number of muons, N , that hit a mirror at sea-level per unit time is expressed as

$$\begin{aligned} N &= 2 \times 10^{-2} \text{ /cm}^2\text{/sec} \times 2R \times H \\ &= 8 \text{ /sec} \left(\frac{2R}{25 \text{ cm}} \right) \left(\frac{H}{15 \text{ cm}} \right). \end{aligned} \quad (42)$$

The average arrival interval of muons, $1/N$, is

$$\frac{1}{N} = 0.13 \text{ sec} \left(\frac{25 \text{ cm}}{2R} \right) \left(\frac{15 \text{ cm}}{H} \right). \quad (43)$$

The decay time of the fundamental resonant vibration is described as

$$\frac{Q_1}{\pi f_1} = 8 \times 10^2 \text{ sec} \left(\frac{40 \text{ kHz}}{f_1} \right) \left(\frac{Q_1}{10^8} \right). \quad (44)$$

Since the Q-values of mirrors used for gravitational wave detectors are at least 10^6 , the decay time is extremely larger than the expected arrival interval of cosmic-ray particles.

B. Power spectral density

The power spectral density, $G_{\text{cos}}(f)$, of vibrations caused by low-energy cosmic-ray particles has been calculated (e.g. Refs. [23, 26]). It is assumed that arrival time of particles and track position in a mirror are at random. Since there are four mirrors in an interferometer, the one-side power spectral density of the noise of an interferometer output is written in the form [56]

$$G_{\text{cos}}(f) = \frac{4}{L^2} \times 8\pi^2 N \langle |\tilde{X}(\omega)|^2 \rangle = \frac{32\pi^2 N}{L^2} \langle |\tilde{X}(\omega)|^2 \rangle, \quad (45)$$

where L is the length of the interferometer arms. The quantity $\langle |\tilde{X}(\omega)|^2 \rangle$ is the ensemble average of $|\tilde{X}(\omega)|^2$, which is the vibration caused by a muon. To evaluate the power spectrum of room-temperature interferometers, the square of Eq. (30) is used as the ensemble average, because this formula is appropriate to calculate the typical $|\tilde{X}(\omega)|$ at 300 K and around 100 Hz, as shown in Sec. III A. From Eqs. (41), (42) and (45), the power spectrum of room-temperature sapphire at sea-level is written as [57]

$$\begin{aligned} \sqrt{G_{\text{cos}}(f)} &= 1.3 \times 10^{-26} \text{ /}\sqrt{\text{Hz}} \left(\frac{3 \text{ km}}{L} \right) \left(\frac{\alpha}{5 \times 10^{-6} \text{ /K}} \right) \\ &\times \left(\frac{1}{2.3} \frac{\sqrt{1-\sigma^2}}{1-2\sigma} \right) \left(\frac{7.9 \times 10^2 \text{ J/kg/K}}{C} \right) \\ &\times \left(\frac{2R}{25 \text{ cm}} \right)^{1/2} \left(\frac{3 \text{ cm}}{r_0} \right)^{1/2} \left(\frac{100 \text{ Hz}}{f} \right). \end{aligned} \quad (46)$$

The sensitivity of future second-generation interferometer projects, such as LCGT [41] and Advanced LIGO [58], is on the order of 10^{-24} / $\sqrt{\text{Hz}}$ at 100 Hz. Therefore, the effect of low-energy cosmic-ray particles is not a serious problem, even in these future projects.

V. APPLICATION II — SHOWER

High-energy cosmic-ray particles often generate many particles (showers). From Eqs. (41) and (63), if 1000 shower particles pass in a mirror at the same time, the excited vibration is large enough to be detected by future second-generation interferometers, such as LCGT [41] and Advanced LIGO [58] (e.g. Refs. [23, 24, 25]). Such excitations caused by cosmic-ray showers have been observed in a resonator [15].

We investigated the effect of a shower generated by a high-energy muon inside a mirror with a Monte-Carlo technique [59]. It was assumed that the material is sapphire. We evaluated the probability that a high-energy muon that runs in a 30 cm thickness sapphire generates more than 1000 electrons. In this simulation, the flux of muons at sea-level was expressed as [61]

$$I_{\mu}(> E) = 1.1 \times 10^{-6} \text{ /cm}^2\text{/sec} \left(\frac{E}{1 \text{ TeV}} \right)^{-2.7}, \quad (47)$$

if E is more than 1 TeV. Our simulation showed that the number per unit time and per a mirror of muons that generate more than 1000 electrons $N(> 1000e)$ is (the typical energy of such muons is about 10 TeV [65])

$$N(> 1000e) = 1.0 \times 10^{-11} / \text{sec} \left(\frac{2R}{25 \text{ cm}} \right) \left(\frac{H}{15 \text{ cm}} \right). \quad (48)$$

It must be noted that this average arrival number, $N(> 1000e)$, was overestimated, because only a part of muons has more than a 30 cm length track in a sapphire mirror. Since there are four mirrors in an interferometer, the average arrival interval is

$$\frac{1}{4N(> 1000e)} = 7.8 \times 10^2 \text{ year} \left(\frac{25 \text{ cm}}{2R} \right) \left(\frac{15 \text{ cm}}{H} \right). \quad (49)$$

The effect of showers generated by high-energy muons inside mirrors is not a serious problem.

In the case of a shower that occurs near a mirror, the energy of an original particle that generates 1000 particles is about 1 TeV [25]. Since the spread of particles in a TeV energy shower is quite large, the typical size mirror of interferometers can not contain all of the energy of a thousand particles. In order to know how often more than 1000 particles go into a mirror, accurate simulations about shower generation in apparatus around mirrors (for example, vacuum chambers and vibration isolation systems) and the response of a mirror are necessary as resonators [66, 67, 68]. This is our future work.

VI. APPLICATION III — EXOTIC-PARTICLE SEARCH

The effect of cosmic-ray particles on gravitational wave detectors suggests that the detectors are useful to search for exotic particles that dissipate a large amount of energy in material. Ideas that resonators can be used as magnetic monopole [19] or mirror dust particle [22] detectors were proposed. The upper limits of the flux of nuclearite [69, 70] from the operation of resonators were reported [20, 21]. Here, we discuss interferometers as exotic-particle detectors in comparison with resonators (bars [6, 7, 8, 9, 10]).

In order to detect exotic particles or other rare events, a larger aperture and higher sensitivity are required for detectors. The cross section of a bar resonator is 10-times larger than that of an interferometer [71]. The area of a bar is about 1.8 m² (diameter, 0.6 m; length, 3 m) [21]. The cross section of four mirrors of an interferometer is about 0.15 m² (diameter, 0.25 m; thickness, 0.15 m). We discuss the sensitivity of interferometers and bars for an exotic particle passage.

A. Signal-to-Noise ratio of interferometers

Since the time evolution of an excited motion by an exotic particle is predicted from Eq. (20), the matched filtering method can be applied to the outputs of detectors. The output of a matched filter, the signal-to-noise ratio (S/N), is defined as [74]

$$S/N = 4\pi \sqrt{\int_0^\infty \frac{|\tilde{S}(\omega)|^2}{G_{\text{det}}(f)} df}, \quad (50)$$

where $\tilde{S}(\omega)$ and $G_{\text{det}}(f)$ are the Fourier components of the signal and the one-side power spectral density of the noise of gravitational wave detectors, respectively.

In the case of interferometers, $G_{\text{det}}(f)$ and $\tilde{S}(\omega)$ of Eq. (50) are the strain noise, $G_{\text{int}}(f)$, and the ratio of the Fourier component of the motion excited by an exotic particle, $\tilde{X}(\omega)$, to the arm length, L , respectively. It is supposed that the temperature is 300 K. Here, we recall Eq. (30) in the form

$$|\tilde{X}(\omega)| \sim \frac{A}{\pi^{3/4}} \frac{\sqrt{1-\sigma^2}}{Y\sqrt{Rr_0}} \frac{1}{f}, \quad (51)$$

$$A = \frac{1}{4\pi^2} \frac{Y\alpha}{1-2\sigma} \frac{1}{\rho C} \frac{dE}{dl}. \quad (52)$$

S/N is expressed by using Eqs. (50) and (51):

$$S/N_{\text{int}} = \frac{4\pi^{1/4} A \sqrt{1-\sigma^2}}{Y\sqrt{Rr_0}L} \sqrt{\int \frac{df}{f^2 G_{\text{int}}(f)}}. \quad (53)$$

B. S/N of bar resonators

In the case of bar detectors, $\tilde{S}(\omega)$ and $G_{\text{det}}(f)$ of Eq. (50) are the force applied by an exotic particle to the n -th mode, $\tilde{F}_n(\omega)$, in Eq. (19), and the tidal force, which corresponds to the strain noise, $G_{\text{bar}}(f)$, respectively. Equation (19) is rewritten as

$$|\tilde{S}(\omega)| = |\tilde{F}_n(\omega)| = A \frac{1}{f} \left(\int \text{div} \mathbf{w}_n dl \right), \quad (54)$$

because the cut-off frequency, $1/(2\pi\tau_n)$, is lower than the resonant frequency. Here, we take the fundamental mode of bars into account. Under the same approximation in the derivation of Eqs. (30) and (34), $\tilde{S}(\omega)$ is expressed as

$$|\tilde{S}(\omega)| = |\tilde{F}_1(\omega)| \sim A \frac{\pi}{\sqrt{2}} \frac{1}{f}. \quad (55)$$

The tidal force that corresponds to the strain noise, $G_{\text{bar}}(f)$, is obtained from Refs. [20, 75, 76],

$$G_{\text{det}}(f) = \left(M_b \omega_{1(b)}^2 \frac{l}{\pi^2} \right)^2 G_{\text{bar}}(f), \quad (56)$$

where M_b , $\omega_{1(b)}$ and l are the mass, angular resonant frequency of the fundamental mode and length of a bar. S/N is given by Eqs. (50), (55), and (56):

$$S/N_{\text{bar}} = \frac{2\sqrt{2}\pi^4 A}{M_b \omega_{1(b)}^2 l} \sqrt{\int \frac{df}{f^2 G_{\text{bar}}(f)}}. \quad (57)$$

C. Comparison between interferometers and bar resonators

Here, we discuss the effects of an exotic particle on interferometers and bar detectors by using Eqs. (53) and (57). The integral term only depends on the sensitivity of gravitational wave detectors. It must be noted that the weight, $1/f^2$, originates from the frequency dependence of $\tilde{S}(\omega)$, i.e. Eqs. (51) and (54). The integral term in Eq. (53) for future second-generation interferometers, e.g. the LCGT project [41], is

$$\sqrt{\int \frac{df}{f^2 G_{\text{int}}(f)}} = 3.0 \times 10^{22}. \quad (58)$$

The typical goal sensitivity of bar resonators [77] is $\sqrt{G_{\text{bar}}(f)} \sim 3 \times 10^{-22} / \sqrt{\text{Hz}}$ in the frequency range between 850 Hz and 950 Hz. The integral term in Eq. (57) is

$$\sqrt{\int \frac{df}{f^2 G_{\text{bar}}(f)}} \sim 3.7 \times 10^{19}. \quad (59)$$

The integral term of interferometers is 1000-times larger, because interferometers have higher sensitivity and a wider observation band. Since the observation band of interferometers is lower than that of resonators, the weighting function, $1/f^2$, increases the integral term of interferometers.

The factors, except for the integral term and A in Eqs. (53) and (57), are the ratios of the responses to an exotic particle to that to the gravitational wave. If this factor is large, the detector is more suitable for exotic-particle searches. This factor of interferometers is [78]

$$\begin{aligned} \frac{4\pi^{1/4} \sqrt{1-\sigma^2}}{Y \sqrt{R} r_0 L} &= 4.9 \times 10^{-14} / \text{N} \left(\frac{\sqrt{1-\sigma^2}}{0.96} \right) \\ &\times \left(\frac{4 \times 10^{11} \text{ Pa}}{Y} \right) \left(\frac{25 \text{ cm}}{2R} \right)^{1/2} \\ &\times \left(\frac{6 \text{ cm}}{r_0} \right)^{1/2} \left(\frac{3 \text{ km}}{L} \right). \end{aligned} \quad (60)$$

In the case of bar resonators, this factor is

$$\begin{aligned} \frac{2\sqrt{2}\pi^4}{M_b \omega_{1(b)}^2 l} &= 1.2 \times 10^{-9} / \text{N} \left(\frac{2300 \text{ kg}}{M_b} \right) \\ &\times \left(\frac{900 \times 2\pi \text{ rad/Hz}}{\omega_{1(b)}} \right)^2 \left(\frac{3 \text{ m}}{l} \right). \end{aligned} \quad (61)$$

The factor of bars is extremely larger. The main reason for this difference comes from the sizes of the detectors, L and l . An exotic-particle detector must be a good displacement sensor. A smaller size detector is a better displacement sensor, if the strain (gravitational wave) sensitivity is the same. The better strain sensitivity of interferometers shown by Eqs. (58) and (59) is canceled by their larger size. The factors in Eqs. (60) and (61), except for L and l , represent the mechanical responses of a mirror and a bar. The response of a bar is typically about 10-times larger.

The amplitude of the force F_n in Eq. (54) is proportional to A . This quantity depends on only the energy loss process of exotic particles and the material of the mirrors and the bar resonators. This is evaluated as

$$\begin{aligned} A &= 7.3 \times 10^{-9} \text{ N} \left(\frac{Y}{4 \times 10^{11} \text{ Pa}} \right) \left(\frac{\alpha}{5 \times 10^{-6} / \text{K}} \right) \\ &\times \left(\frac{0.42}{1-2\sigma} \right) \left(\frac{7.9 \times 10^2 \text{ J/kg/K}}{C} \right) \\ &\times \left(\frac{1}{3 \text{ GeV}/(\text{g cm}^{-2})} \frac{1}{\rho} \frac{dE}{dl} \right). \end{aligned} \quad (62)$$

In the quantities of Eq. (62), only the linear thermal-expansion coefficient, α , strongly depends on the material [79]. The values of the coefficient α for fused silica and sapphire at 300 K, are $5.5 \times 10^{-7} / \text{K}$ and $5.0 \times 10^{-6} / \text{K}$, respectively. The coefficient α of the alloy Al5056 [80], which is the most popular material of bar resonators [6, 7, 8, 9], is $2.3 \times 10^{-5} / \text{K}$.

From the above discussion, the advantages of interferometers, the higher strain sensitivity and wider observation band, are canceled by their larger detector size, because exotic-particle detectors must have good displacement sensitivity, not strain sensitivity. The larger mechanical response (about 10 times) and linear thermal-expansion coefficient (several or several tens times) of bar resonators enhance the sensitivity. The typical S/N of interferometers is obtained from Eqs. (53), (58), (60), and (62):

$$\begin{aligned} S/N_{\text{int}} &= 10^1 \left(\frac{\alpha}{5.0 \times 10^{-6} / \text{K}} \right) \\ &\times \left(\frac{1}{3 \text{ GeV}/(\text{g cm}^{-2})} \frac{1}{\rho} \frac{dE}{dl} \right). \end{aligned} \quad (63)$$

The S/N of bar resonators is evaluated from Eqs. (57), (59), (61), and (62):

$$\begin{aligned} S/N_{\text{bar}} &= 3 \times 10^2 \left(\frac{\alpha}{2.3 \times 10^{-5} / \text{K}} \right) \\ &\times \left(\frac{1}{3 \text{ GeV}/(\text{g cm}^{-2})} \frac{1}{\rho} \frac{dE}{dl} \right). \end{aligned} \quad (64)$$

The sensitivity for an exotic particle of bars is a few tens or a few hundreds times better than that of interferometers [81]. The sensitivity of bars in the above discussion,

Eq. (59), is based on the goal sensitivity. The current sensitivity is 10-times worse than it [77]. The current bar resonators are the better exotic-particle detectors than the future second-generation interferometers as LCGT [41] and Advanced LIGO [58].

It is difficult to improve the sensitivity of interferometers for exotic particles. One reason is that in order to enhance the signal, the mechanical response and the coefficient of thermal expansion of a mirror must be larger. Equation (60) implies that a smaller mirror and beam yield a larger mechanical response. However, this strategy enhances the amplitude of the displacement noise, and the S/N does not increase. A smaller mirror increases the radiation-pressure noise ($\propto R^{-3}$). A smaller beam and a larger coefficient of thermal expansion increase the amplitude of the thermal noise caused by thermoelastic damping in the mirror substrate ($\propto \alpha/r_0^{3/2}$) [83]. Although mirror cooling reduces the thermal noise [45, 46, 47], S/N does not become larger, because the excitation by an exotic particle becomes smaller than that at room temperature, as shown in Sec. III A.

VII. CONCLUSIONS

We obtained a general formula for a mirror vibration caused by a cosmic-ray particle, and studied the effects in typical cases of interferometric experiments. This formula reveals differences in the responses of resonators and interferometers against cosmic-ray particles. In the case of resonators, the contribution of the resonant vibration is dominant. On the contrary, in the case of interferometers, the motion of the centers of resonant vibrations must be taken into account. Although the effect of cosmic-ray particles of resonators is independent

of the temperature, in the case of interferometers, vibrations caused by cosmic-ray particles can be reduced by using cooling mirrors. In the case of bar resonators, the particle track position dependence of the vibration by a cosmic-ray particle is symmetric with respect to the center of a resonator, as shown in Fig. 4. On the other hand, in interferometers, larger motion is observed if the track is near the laser beam spot on the surface of a mirror.

The typical vibration amplitude of interferometers caused by cosmic-ray particles was evaluated. The power spectrum of vibrations by low-energy cosmic-ray muons (less than 100 GeV) is about 100-times smaller than the goal sensitivity of the future second-generation projects, such as LCGT and Advanced LIGO. The arrival frequency of high-energy cosmic-ray muons that generate enough large showers inside the mirrors of LCGT and Advanced LIGO is one per a millennium. If a shower that occurs near a mirror brings more than a thousand particles to the mirror (an original particle of the shower has an energy that is more than 1 TeV), the vibration will be observed in LCGT and Advanced LIGO interferometers. A detailed study on such shower events is our future work. We also discussed the possibility of a use of gravitational wave detectors for exotic-particle searches. Interferometers and bar resonators were compared as detectors for such an exotic-particle search. The cross section of bars is 10-times larger than that of interferometers. The sensitivity of bars for an exotic particle is (30 \sim 300) times better than that of interferometers.

Acknowledgments

We are grateful to Jun Nishimura for useful comments.

-
- [1] A. Abramovici *et al.*, *Science* **256**, 325 (1992).
 - [2] C. Bradaschia *et al.*, *Nucl. Instrum. Methods Phys. Res., Sect. A* **289**, 518 (1990).
 - [3] B. Willke *et al.*, *Class. Quant. Grav.* **19**, 1377 (2002).
 - [4] M. Ando *et al.*, *Phys. Rev. Lett.* **86**, 3950 (2001).
 - [5] S. Miyoki *et al.*, *Class. Quant. Grav.* **21**, S1173 (2004).
 - [6] E. Mauceli *et al.*, *Phys. Rev. D* **54**, 1264 (1996).
 - [7] E. Amaldi *et al.*, *Nuovo Cimento* **7C**, 338 (1984); **9C**, 829 (1986).
 - [8] P. Astone *et al.*, *Astropart. Phys.* **7**, 231 (1997).
 - [9] M. Bonaldi *et al.*, *Physica B* **194-196**, 1 (1994); M. Cerdonio *et al.*, *Physica B* **194-196**, 3 (1994).
 - [10] D.G. Blair *et al.*, *Phys. Rev. Lett.* **74**, 1908 (1995).
 - [11] O.D. Aguiar *et al.*, *Class. Quant. Grav.* **19**, 1949 (2002).
 - [12] B.L. Beron and R. Hofstadter, *Phys. Rev. Lett.* **23**, 184 (1969).
 - [13] A.M. Grassi Strini, G. Strini, and G. Tagliaferri, *J. Appl. Phys.* **51**, 948 (1980).
 - [14] G.D. van Albada *et al.*, *Rev. Sci. Instrum.* **71**, 1345 (2000).
 - [15] P. Astone *et al.*, *Phys. Rev. Lett.* **84**, 14 (2000).
 - [16] P. Astone *et al.*, *Phys. Lett. B* **499**, 16 (2001).
 - [17] P. Astone *et al.*, *Phys. Lett. B* **540**, 179 (2002).
 - [18] M. Bassan *et al.*, *Europhys. Lett.* **76**, 987 (2006).
 - [19] C. Bernard, A. De Rújula, and B. Lautrup, *Nucl. Phys. B* **242**, 93 (1984).
 - [20] G. Liu and B. Barish, *Phys. Rev. Lett.* **61**, 271 (1988).
 - [21] P. Astone *et al.*, *Phys. Rev. D* **47**, 4770 (1993).
 - [22] R. Foot and S. Mitra, *Phys. Rev. D* **68**, 071901(R) (2003).
 - [23] A. Giazotto, *Phys. Lett. A* **128**, 241 (1988).
 - [24] R.W. Clay, A.G.K. Smith, and J.L. Reid, *Publ. Astron. Soc. Aust.* **14**, 195 (1997).
 - [25] V.B. Braginsky, O.G. Ryazhskaya, and S.P. Vyatchanin, *Phys. Lett. A* **350**, 1 (2006).
 - [26] V.B. Braginsky, O.G. Ryazhskaya, and S.P. Vyatchanin, *Phys. Lett. A* **359**, 86 (2006).
 - [27] A. Marin, in *Proceedings of the 2nd Gravitational Wave Data Analysis Workshop, Orsay, France, 1997*, edited by M. Davier and P. Hello (Editions Frontiers, Orsay, France, 1998), p. 193.
 - [28] R.M. Sternheimer, M.J. Berger, and S.M. Seltzer, *Atom.*

- Data Nucl. Data Tables **30**, 261 (1984).
- [29] D.E. Groom, N.V. Mokhov, and S.I. Striganov, *Atom. Data Nucl. Data Tables* **78**, 183 (2001).
- [30] L.D. Landau and E.M. Lifshitz, *Theory of Elasticity* (Pergamon, New York, 1986), Chaps. 1, 3, 5. The quantity C in this reference is ρC of this paper. The quantity α in this reference is the volumetric thermal-expansion coefficient, which is three-times larger than the linear thermal expansion, α , in this paper.
- [31] Equation (3.14) of Ref. [19]. The quantity α in Ref. [19] is $\kappa/(\rho C)$ in this paper.
- [32] P.R. Saulson, *Phys. Rev. D* **42**, 2437 (1990).
- [33] K. Yamamoto, Ph.D. thesis, The University of Tokyo, 2001 (http://t-munu.phys.s.u-tokyo.ac.jp/theses/yamamoto_d.pdf).
- [34] K. Yamamoto, M. Ando, K. Kawabe, and K. Tsubono, *Phys. Rev. D* **75**, 082002 (2007).
- [35] R.M. Marinho, Jr., N.S. Magalhães, O.D. Aguiar, and C. Frajuca, *Phys. Rev. D* **64**, 065017 (2001).
- [36] Our result concerning the force $F_n(0)$ agrees with that derived from δE_n , which is equal to $F_n^2/(2m_n\omega_n^2)$ in Eq. (2) of Ref. [20]. The quantity C_p in Eq. (2) of Ref. [20] is ρC in this paper. It must be noted that M in Eq. (2) of Ref. [20] is the mass of a mirror, not the effective mass, m_n . This discrepancy is canceled by the difference of the normalized condition of the basis functions, w_n . In this paper, the normalized condition is Eq. (11). In Ref. [20], the normalized condition is the same as Eq. (5.6) of Ref. [19].
- [37] A. Gillespie and F. Raab, *Phys. Rev. D* **52**, 577 (1995).
- [38] F. Bondu and J.-Y. Vinet, *Phys. Lett. A* **198**, 74 (1995).
- [39] F. Bondu, P. Hello, and J.-Y. Vinet, *Phys. Lett. A* **246**, 227 (1998).
- [40] This formula is valid if the mirror thickness is comparable to the mirror radius, and the beam radius is extremely smaller than the mirror radius.
- [41] K. Kuroda *et al.*, *Prog. Theor. Phys. Suppl.* **163**, 54 (2006).
- [42] Einstein Telescope (ET) is a future third-generation project in Europe. The interferometer has vacuum tubes, of which the total length is 30 km, and cryogenic mirrors. The details of the design are presently being discussed (H. Lück, private communications).
- [43] The super-conductive transition changes, dE/dl [16, 17, 18]. Such a case is not considered because the mirror material does not generally become a superconductor.
- [44] Problem 5 of Chapter 5 in C. Kittel, *Introduction to Solid State Physics* (John Wiley & Sons, Inc., New York, 1986).
- [45] T. Uchiyama *et al.*, *Phys. Lett. A* **261**, 5 (1999).
- [46] T. Uchiyama *et al.*, *Phys. Lett. A* **273**, 310 (2000).
- [47] K. Yamamoto *et al.*, *Phys. Rev. D* **74**, 022002 (2006).
- [48] T. Tomaru *et al.*, *Class. Quant. Grav.* **19**, 2045 (2002).
- [49] K. Yamamoto *et al.*, in *Proceedings of the 7th Edoardo Amaldi Conference on Gravitational Waves, Sydney, Australia, 2007*; *J. Phys.: Conf. Ser.* **122** 012015 (2008) (Institute of Physics, Bristol, United Kingdom).
- [50] The results of the discussion presented in this section are valid under arbitrary normalization conditions [34]. The right-hand sides of Eqs. (8) and (10) in a general case are $\sum_n q_n(t) \int w_{n,\text{opt}}(\mathbf{r})P(\mathbf{r})dS$ and $\tilde{F}_n / \int w_{n,\text{opt}}(\mathbf{r})P(\mathbf{r})dS$, respectively. The signs of $q_n(t) \int w_{n,\text{opt}}(\mathbf{r})P(\mathbf{r})dS$ and $\tilde{F}_n / \int w_{n,\text{opt}}(\mathbf{r})P(\mathbf{r})dS$ cancel out each other in the process of the calculation for \tilde{X} .
- [51] Yu. Levin, *Phys. Rev. D* **57**, 659 (1998).
- [52] A.M. Hillas, *Cosmic Rays*, (Pergamon Press, New York, 1972).
- [53] P.K.F. Grieder, *Cosmic Rays at Earth*, (Elsevier, Amsterdam, 2001).
- [54] T.K. Gaisser, *Cosmic Rays and Particle Physics*, (Cambridge University Press, Cambridge, England, 1990).
- [55] M.S. Longair, *High Energy Astrophysics Vol.I*, (Cambridge University Press, Cambridge, England, 1992).
- [56] In this paper, the one-side power spectral density $G_Y(f)$ is defined as $\lim_{T \rightarrow \infty} 8\pi^2 \left\langle \left| \int_{-T/2}^{T/2} Y(t) \exp(-i\omega t) dt / (2\pi) \right|^2 \right\rangle / T$. The integral $\int_0^\infty G_Y(f) df$ is the average of $|Y(t)|^2$, $\lim_{T \rightarrow \infty} \int_{-T/2}^{T/2} \langle |Y(t)|^2 \rangle dt / T$ (Parseval's theorem).
- [57] It must be remembered that Eq. (30) is an approximation formula under the condition that the mirror radius, R , is comparable to its height, H .
- [58] P. Fritschel, in *Proceedings of the SPIE meeting Gravitational-Wave Detection (4856-39)*, Waikoloa, Hawaii, 2002, edited by P. Saulson and M. Cruise (International Society for Optical Engineering, WA, 2002), p. 282.
- [59] The details of the Monte-Carlo simulation are as follows. The energy of muons is dissipated via three processes: bremsstrahlung (photon emission from charged particles accelerated by the Coulomb potential of nuclei), direct electron-pair production and interactions with nuclei [54]. Photons and electron-positron pairs originating from these processes generate electromagnetic cascades. In order to simplify the simulation, secondary particles generated in the interactions between muons and nuclei were replaced by a gamma-ray photon. Since the interactions with nuclei are rather rare compared to the other two processes mentioned above, this simplification did not have a serious effect on the results. In the process of the electromagnetic cascade, the bremsstrahlung and ionization of electrons and the electron-positron creation by photons were taken into account. Our simulation about an electromagnetic cascade from an electron agreed with the result shown in Ref. [60]. Moreover, the result of this Monte-Carlo simulation was consistent with the formula of the averaged energy dissipation of a high-energy muon (more than about 1 TeV) in sapphire [29, 54], $dE/dl = 8 \text{ MeV/cm } [E/(700 \text{ GeV})]$. It was assumed that sapphire consists of a kind of atom. It had $Z^2 = 10.3^2$ (square of atomic number) and $A = 21$ (mass number) which are the averages of those of Al_2 and O_3 .
- [60] B. Rossi and K. Greisen, *Rev. Mod. Phys.* **13**, 240 (1941).
- [61] In order to evaluate this expression, we used a standard muon intensity at sea-level given by Gaisser [54] (equation (3) and the original Gaisser parameterization in Ref. [62]). The zenith angle dependence of this muon intensity was evaluated taking into account the radius of the Earth (6367.5 km) and the thickness of the atmosphere (32 km) as Fig. 12 of Ref. [63]. In order to check our calculation, we considered another formula about the zenith angle distribution, Eq. (10) in Ref. [64]. We obtained the almost same result.
- [62] A. Tang, G. Horton-Smith, V.A. Kudryavtsev, and A. Tonazzo, *Phys. Rev. D* **74**, 053007 (2006).
- [63] Y. Muraki *et al.*, *Phys. Rev. D* **28**, 40 (1983).
- [64] A. Okada, *Astropart. Phys.* **2**, 393 (1994).

- [65] From our simulation, a 10 TeV muon does not usually generate 1000 electrons after it runs in the 30 cm thickness sapphire. In the average case, the electron number increases until the muon track length in the sapphire reaches 150 cm. In the stationary state after a 150 cm run, the average electron number is about 10 for the case of a 10 TeV muon (this average electron number in the stationary state is proportional to the muon energy).
- [66] F. Ricci, Nucl. Instrum. Methods Phys. Res., Sect. A **260**, 491 (1987).
- [67] J. Chiang, P. Michelson, and J. Price, Nucl. Instrum. Methods Phys. Res., Sect. A **311**, 603 (1992).
- [68] E. Coccia *et al.*, Nucl. Instrum. Methods Phys. Res., Sect. A **355**, 624 (1995).
- [69] E. Witten, Phys. Rev. D **30**, 272 (1984).
- [70] A. De Rújula and S.L. Glashow, Nature **312**, 734 (1984).
- [71] There are exotic-particle detectors that have larger cross sections than those of bar resonators. For example, the total cross section of the MACRO detector is about 1000 m² [72, 73].
- [72] M. Ambrosio *et al.*, Eur. Phys. J. C **13**, 453 (2000).
- [73] A. Kumar *et al.*, Radiat. Meas. **36**, 301 (2003).
- [74] L.S. Finn and D.F. Chernoff, Phys. Rev. D **47**, 2198 (1993).
- [75] H. Hirakawa, K. Narihara, and M.-K. Fujimoto, J. Phys. Soc. Jpn. **41**, 1093 (1976).
- [76] Since the result depends on the Poisson ratio weakly, it is supposed that this quantity is zero.
- [77] A. Vinante *et al.*, Class. Quant. Grav. **23**, S103 (2006).
- [78] In order to reduce the thermal noise below the goal sensitivity of the future second-generation interferometers without mirror cooling, the beam radius must be larger than the typical value 3 cm. In Advanced LIGO [58], the beam radius is 6 cm.
- [79] The loss of monopoles in conductors is different from that in insulators, because the former is dominated by the eddy-current dissipation [19]. Such a case is not considered because the mirror material of the interferometric gravitational wave detectors is not usually a conductor.
- [80] T. Suzuki, K. Tsubono, and H. Hirakawa, Phys. Lett. **67A**, 2 (1978).
- [81] The scintillators and track-etch detectors (e.g. CR39) [21, 72, 73, 82] have a sensitivity that is comparable to that of bar resonators. From Eq. (64) and Ref. [70, 72], these apparatus find exotic particles, even if the energy loss $(1/\rho)dE/dl$ is on the order of 10 MeV/(g cm⁻²).
- [82] S. Nakamura *et al.*, Phys. Lett. B **263**, 529 (1991).
- [83] V.B. Braginsky, M.L. Gorodetsky, and S.P. Vyatchanin, Phys. Lett. A **264**, 1 (1999).